Is the knowledge of the surface topology and contact angles enough to define the drop impact outcome?

Ileana Malavasi,[1] Federico Veronesi,[2] Aurora Caldarelli,[2] Maurizio Zani,[3,4] Mariarosa Raimondo,[2] Marco Marengo[1,5*]

[1] Department of Engineering and Applied Sciences, University of Bergamo, Viale Marconi 5, 24044 Dalmine (BG), Italy.

[2] ISTEC CNR - Institute of Science and Technology for Ceramics, Via Granarolo 64, 48018 Faenza (RA), Italy.

[3] Department of Physics, Politecnico di Milano, Piazza Leonardo da Vinci 32, 20133 Milano, Italy.

[4] Center for Nano Science and Technology @Polimi, Istituto Italiano di Tecnologia (IIT), Via G. Pascoli 70/3, 20133 Milano, Italy.

[5] School of Computing, Engineering and Mathematics, University of Brighton, Lewes Road, BN2 4GJ, Brighton, UK.

ABSTRACT: It is well known that a superhydrophobic surface may not be able to repel impacting droplets due to the so-called Cassie-to-Wenzel transition. It has been proven that a critical value of the receding contact angle (θ_R) exists for the complete rebound of water, recently experimentally measured to be 100° for a large range of impact velocities. On the contrary, in the present work, no rebound was observed when low surface tension liquids such as hexadecane (σ = 27.5 mN/m at 25°C) are concerned, even for very low impact velocities and very high values of θ_R and low contact angle hysteresis. Therefore, the critical threshold of $\theta_R \approx 100°$ does not sound acceptable for all liquids and for all the hydrophobic surfaces. For the same Weber numbers a Cassie-to-Wenzel state transition occurs after the impact due to the easier penetration of low surface tension fluids in the surface structure. Hence a criterion for drop rebound of low surface tension liquids must consider not only the contact angle values with surfaces, but also their surface tension and viscosity. This suggests that, even if it is possible to produce surfaces with an enhanced static repellence against oils and organics, generally the realization of synthetic materials with remaining self-cleaning and anti-sticking abilities in dynamic phenomena, such as spray impact for example, still remains an unsolved task. Moreover, it is demonstrated that also the chemistry of the surface and the physico-chemical interactions with the liquid drops and the possible wettability gradient of the surface asperity play an important role in determining the critical Weber number above which impalement occurs. Therefore the classical numerical simulations of drop impacts onto dry surfaces are definitively not able to capture the final outcomes of the impact for all the possible fluids, if the surface topology and chemistry and/or the wettability gradient in the surface structure are not properly reflected.

INTRODUCTION

The impact of drops onto dry solid surfaces is a phenomenon involved in many industrial applications, i.e. spray cooling, ink-jet printing, spray painting, fuel injection, raindrop erosion, etc. The investigation of the single drop impact[1-3] is the first step toward the understanding and the control of the liquid–solid interactions in complex phenomena where the capillarity, the viscous forces and the impact momentum play a key role. In the last decade, notwithstanding the open issue of their durability[4], superhydrophobic surfaces (SHS) have attracted an increasing interest in both the academic and industrial sectors, due to their remarkable self-cleaning and anti-sticking properties[5-7], involving a wide range of potential applications: biomedical[8-9], microfluidic[10], corrosion resistance[11], drag reduction[12], anti-icing[13], contamination and oxidation protection[14], etc. SHS are highly hydrophobic surfaces on which liquid water adhesion is very low, therefore resulting extremely difficult to be wetted. Superhydrophobicity causes the water droplet to bead up on the surface instead of spreading on it. In addition, capillary adhesion forces are low and water drops typically preserve a high mobility on the surface. The wetting behavior is evaluated by the contact angle occurring when a liquid/vapor interface meets the solid surface. In this work, advancing (θ_A or ACA) and receding (θ_R or RCA) contact angles were measured, respectively, by expanding and contracting water and hexadecane sessile drops on a horizontal surface (sessile drop method). In static conditions, θ_A and θ_R are, respectively, the maximum and the minimum stable angles. Both of them provide the range of contact angles at equilibrium, while their difference $\Delta\theta = \theta_A - \theta_R$ - named as contact angle hysteresis (CAH) - provides an indication of the drop mobility (the lowest the $\Delta\theta$ value, the highest the drop mobility). As reported in the literature, the

standard conditions are $\theta_R > 135°$ and $\Delta\theta < 10°$ for superhydrophobicity[4], $\theta_A > 90°$ for hydrophobicity and $\theta_A < 90°$ for hydrophilicity[15]. A surface able to repel liquids with a different polarity and physical properties (i.e. surface tension) is called amphiphobic or lyophobic[16-20], with both terms being usually related to the liquids molecules and not to the surfaces. Such particular non-wetting surfaces can provide additional performances with respect to the hydrophobic ones in many sectors. Similarly, superamphiphobic surfaces exhibit even larger values of static contact angles and CAH lower than 5°. Different approaches can be used to achieve these surface properties. For recent trends in the development, fabrication, and characterization of superamphiphobic surfaces, the papers of Cavalli and Mugele[16], Chua and Seeger[20] give useful insights. Throughout the impact on such surfaces, the drop mobility is related to a sort of "dynamic superamphiphobicity", defined as the critical wetting value under which an impacting drop with a given impact velocity does not wet the surface, i.e. a complete drop rebound is observed. In this case the impact velocity, the interfacial tension, the viscosity of the liquid, the chemical and physical properties of the surface determine the drop outcome as well as the spreading and the retraction dynamic. Nonetheless, a few papers[21-23] have shown how superamphiphobic surfaces might not necessarily lead to a total rebound of impinging water drops, especially above a given value of Weber number ($We = \rho v^2 D_o/\sigma$, where ρ is the density of the fluid [kg/m^3], v is its impact velocity [m/s], D_o is the droplet diameter [m] and σ is the surface tension [N/m]). Eventually impalement can occur, leading to the droplet deposition on the surface. In this sense a surface only hydrophobic, but smoother or with a proper topology can be more effective in repelling liquids even for a large value of We. Recently Antonini et al.[21] analyzed the drop impact on horizontal surfaces and highlighted the role of the θ_R on the drop rebound. Accordingly, the rebound can be observed only on surfaces presenting θ_R greater than 100° with the rebound time decreasing as θ_R increases. However, Antonini et al. only refer to water as impacting liquid[21].

To better understand the existence of a general criterion to predict the drop impact outcome, and the key parameters governing the drop-surface interaction, the normal impact of both water and hexadecane drops on solid dry surfaces with different wettability was observed using a high-speed camera. The wetting behavior of sandblasted aluminum foils before (TQ sample) and after the deposition of: i) organic-inorganic hybrid coatings (S samples), ii) infused hybrid coatings (SI samples), iii) grafting fatty acid treatments (LAU) and iv) grafting FAS (FAS) has been analyzed. The present study aims at establishing a relationship between drop impact outcomes and the different parameters for both the liquid drop (impact velocity, surface tension, viscosity) and the solid surface (morphology and roughness, chemistry, wettability).

EXPERIMENTAL SECTION

Surface fabrication – Four kinds of SHS have been prepared: S, SI, LAU and FAS. Moreover, the uncoated sandblasted aluminum surface taken as reference is named TQ. S samples were prepared by dip-coating aluminum foils in an aqueous alumina sol with average particle size of about 30 nm. After thermal treatments, also including boiling in deionized water, a nanostructured inorganic coating was obtained, which was then further functionalized by dipping in a commercial solution of fluoroalkylsilane in isopropanol (Dynasylan® SIVO CLEAR EC, Evonik), resulting into a hybrid organic-inorganic coating. More details on the fabrication of S samples were reported by Raimondo et al. in a previous work[24]. SI samples were obtained by the same route, with an additional step of immersion into a fluorinated lubricant (Fluorinert™ FC-43, 3M™) allowing for the formation of a continuous liquid film on the material surface with the aim of changing the physical nature of the interface (from the solid-liquid-air of S samples to the liquid-liquid-air of SI ones, according to the so-called SLIPS approach[25-26]). Fatty acid surfaces (LAU) were fabricated on an aluminum substrate, previously etched in acid solution, to achieve the desired surface roughness, and subsequently grafted in an ethanol lauric acid solution[4]. FAS surfaces were fabricated by etching the surface in acid solution as for the LAU surface, and then functionalized in a water solution of perfluoroctyltriethoxysilane (FAS)[27].

Surface characterization - The average values of θ_A, θ_R and CAH with both water and hexadecane are reported in Figure 1. The contact angle θ was calculated automatically from drop images by measuring the tangent of a circle fitting the drop profile at the contact point (OCA 15, Data Physics Instr.). Typical drop volume was about 2 µl.

Surfaces have also been characterized in terms of topography and roughness. SEM images were obtained with a Tescan MIRA3 equipment, while roughness measurements were performed with a ContourGT-K (Bruker Nano GmbH) optical profilometer (vertical resolution < 0.01 nm, lateral resolution 0.38 µm). SEM images of S and SI surfaces (Figure 2) show a flower-like nanostructure made up of crossed, 200 nm long flakes and nanometric cavities. Previous results[24] proved that such structure is due to the γ-alumina coating obtained by deposition of Al_2O_3 nanoparticles and to the subsequent boiling in water. LAU and FAS samples display a terrace-like structure with sub-micrometric edges, as expected from the similar etching conditions held for both samples. On the sandblasted TQ surface taken as a reference, microabrasion by sand grains produced an irregular microstructure with asperities and cavities. Roughness data (S_a, S_q, S_v and S_z)[28] are

shown in Figure 3. S_a defines the average of the absolute values of the profile heights Z (x,y) in the measured area, while S_q is the root mean squared of Z (x,y) in the measured area. S_v expresses the maximum value of "valley" depth on the surface in the measured area and S_z expresses the sum of the maximum value of peak height and the maximum value of valley depth on the surface within the measured area. A 15x15mm² area was analyzed for every measure, and a minimum of three measurements were done on the same sample for repeatability reason. The difference between coated (S, SI) and etched (LAU, FAS) samples can be remarked: the former have lower average roughness (S_a, S_q) but higher peaks (S_v, S_z). A comparison with the data obtained for a TQ surface led us to conclude that the hybrid nanostructured coating has a small influence on the micrometric roughness of S and SI, while the main contribution belongs to the microstructure provided by sandblasting. On LAU and FAS surfaces, etching provided a rougher structure, but with less pronounced asperities and cavities.

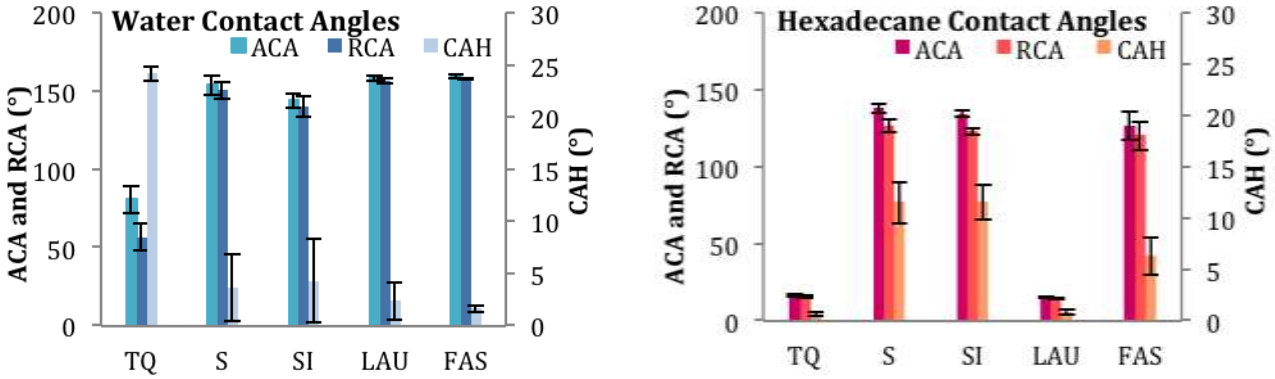

Figure 1. Average advancing (ACA) and receding contact angles (RCA) and contact angle hysteresis (CAH) with water (left) and hexadecane (right).

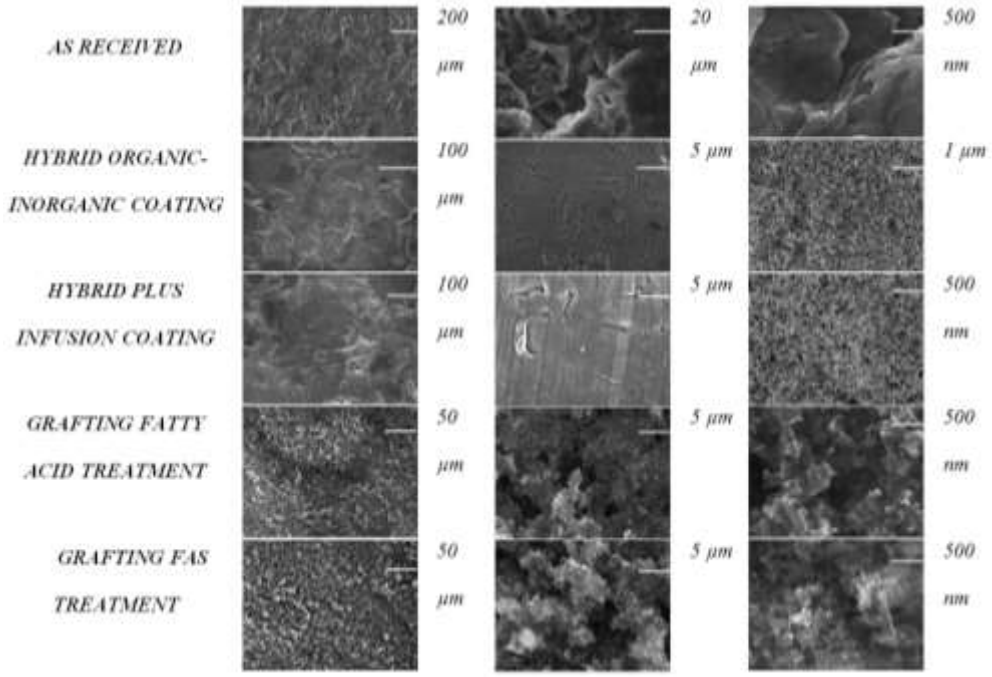

Figure 2. SEM images of the sample surfaces: as received sandblasted (TQ), hybrid organic-inorganic coating (S), hybrid plus infusion coating (SI), grafting fatty acid treatment (LAU) and grafting FAS treatment (FAS).

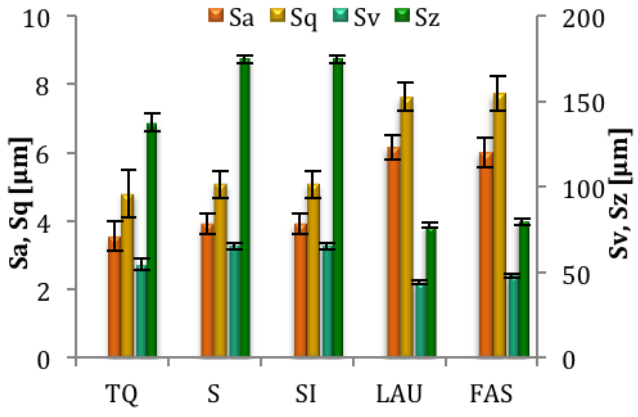

Figure 3. Surface roughness data obtained on TQ, S, SI, LAU and FAS samples. S_a and S_q values are referred to the left vertical axis, while S_v and S_z are referred to the right vertical axis.

Drop impact experiments - A typical experimental apparatus for drop impact studies was used: a drop was generated at the tip of a hydrophobic needle, and then was accelerated by gravity and impacted onto a dry, solid surface. Experimental conditions were the following: impact speed in the $0.05 < V < 4.2$ m/s range, drop diameter in the $1.5 < D_0 < 2.6$ mm range, Weber numbers in the $0.1 < We < 635$ range, and Ohnesorge number ($Oh = \mu/(\rho\sigma D_0)^{1/2}$, where μ is the liquid viscosity [Pa s]) in the $0.0023 < Oh < 0.0186$ range. Images of drop impacts were recorded using a high-speed camera (PCO 1200-HS) with typical frame rates of 1568 and 2477 fps and a pixel resolution of 31 µm/pixel. Tests were repeated at least 10 times for each condition to assess experimental reproducibility. Images were manually analyzed to identify the drop impact outcome and eventually to measure the time of the drop rebound when occurring.

RESULTS AND DISCUSSION

In Table 1 and in Figure 4 the summary of all the outcomes of the drop impact tests is reported. Five main regimes stand out: complete rebound, partial rebound, prompt splash, receding breakup and deposition. All the functionalized surfaces are able to generate a complete or partial rebound of water drops, while TQ surface promotes drop deposition for We up to about 200 and receding break-up for higher Weber numbers. Remarkably, surfaces S and SI are able to repel the water drops up to the maximum We value of 620. No splash is observed for the entire range of We, confirming the previous literature results[29]. In the case of hexadecane, no rebound was observed for any of the surfaces, even if the contact angles and the hysteresis reached, respectively, very high and very low values (i.e. FAS surface, see Figure 1). The prompt splash appears to be an important outcome for $We > 200$. FAS sample shows a peculiar behavior, since it produces a partial rebound with water even for moderate values of We, while with hexadecane it is able to allow the generation of a singular jet[30] for very low We, and allows the receding breakup behavior for the higher analyzed We.

Image sequences of water and hexadecane liquid drops normally impacting on the tested surfaces are shown in Figures 5 and 6, respectively. Interestingly, when a water drop impacts on TQ at $We \approx 21$, deposition occurs with the generation of a singular jet[30], as shown in Figure 7. The same behavior can be observed in the case of hexadecane drop impacting on FAS surface at $We \approx 15$.

A schematic representation of the drop impact test outcome is reported in Figure 4.

Table 1. Summary of the outcomes of the drop impact tests. R = rebound, PR = partial rebound, PS = prompt splash, RB = receding breakup, D = deposition. *Singular jet. ** Transition region.

	We (WATER)							We (HEXADECANE)						
Surface type	< 1.5	16 ÷35	40 ÷75	65 ÷100	150 ÷215	270 ÷360	500 ÷620	10 ÷20	30 ÷40	60 ÷75	85 ÷125	205 ÷275	325 ÷485	545 ÷635
TQ	D	D*	D	D	D	RB	RB	D	D	D	D	D	PS	PS
S	R	R	R	R	R	R	R	D	D	D	D	PS	PS	PS
SI	R	R	R	R	R	R	R	D	D	D	D	PS	PS	PS
LAU	R	R	R	R	R	R	PR	D	D	D	D	D	PS	PS
FAS	R	R	R	R	PR/R**	PR	PR	D*	D	D/RB**	D/RB**	D/RB**	RB	RB

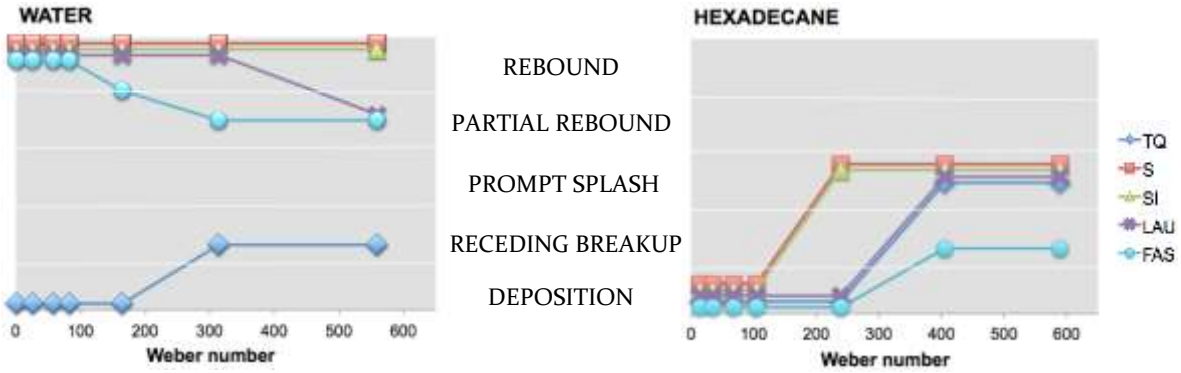

Figure 4. Schematic representation of the drop impact test outcome. In the graphs, the mean values of each We interval are reported.

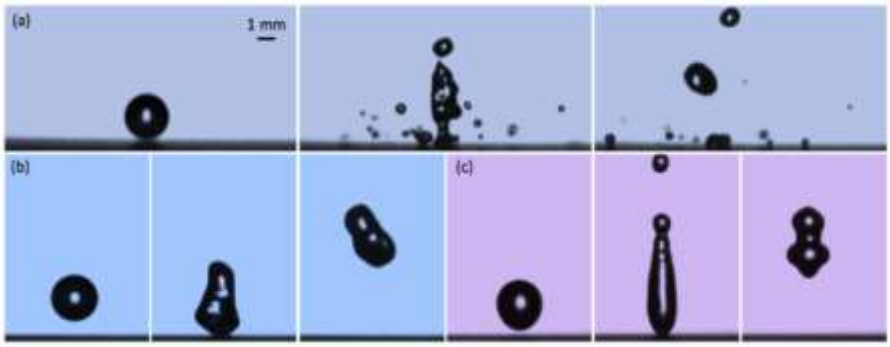

Figure 5. Image sequences of water drops (average diameter D_o = 2.45 mm) impacting on three functionalized surfaces: (a) partial rebound with fragmentation on FAS sample at We = 312 at t = 0, 14.6 ms and 31.2 ms after impact; (b) rebound on SI sample at We = 54 at t = 0, 11.5 ms and 31.2 ms after impact; (c) rebound on S sample at We = 21 at t = 0, 14.0 ms and 21.6 ms after impact. The scale bar in (a) is valid for all images.

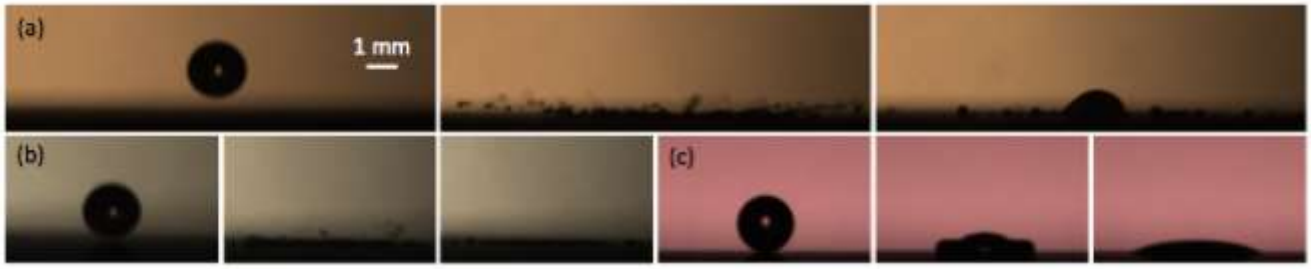

Figure 6. Image sequences of hexadecane drops (average diameter D_o = 1.66 mm) impacting on three functionalized surfaces displaying different behavior: (a) receding breakup on FAS sample at We = 560; (b) splash on SI sample at We = 580; (c) deposition on LAU sample at We = 17. For every surface, images at t = 0, 2.0 ms and 17.6 ms after impact are reported. The scale bar in (a) is valid for all images.

Figure 7. Image sequence of water drop (average diameter D_o = 2.35 mm) impacting on TQ surface at We = 21. A deposition occurs with the generation of a secondary drop. The scale bar in the first frame is valid for all images.

The evolution of the spreading film diameter of water and hexadecane after the instant of impact is shown in Figures 8a and 8b, respectively. The dimensionless diameter of the spreading film, called the spread factor, $\xi(t) = D(t)/D_o$ (i.e., the contact diameter at time t, made dimensionless by dividing it for the initial drop diameter) is shown as function of time. Different outcomes were observed from deposition to rebound (occurring for t>0 when $\xi = 0$). In SHS cases, drops do not stick on the surface and the rebounds of the droplets can be observed. When the drop is detached from the surface, the contact diameter is zero, therefore the spread factor is zero. The time evolution of the spread factor suggests that the drop impact dynamics depends not only on the θ_R value, since, contrary to what reported by Antonini et al.[21], even when θ_R reaches 120° indicating a very low wettability, complete drop rebound does not occur (see tests with hexadecane on FAS surfaces, Figure 8b).

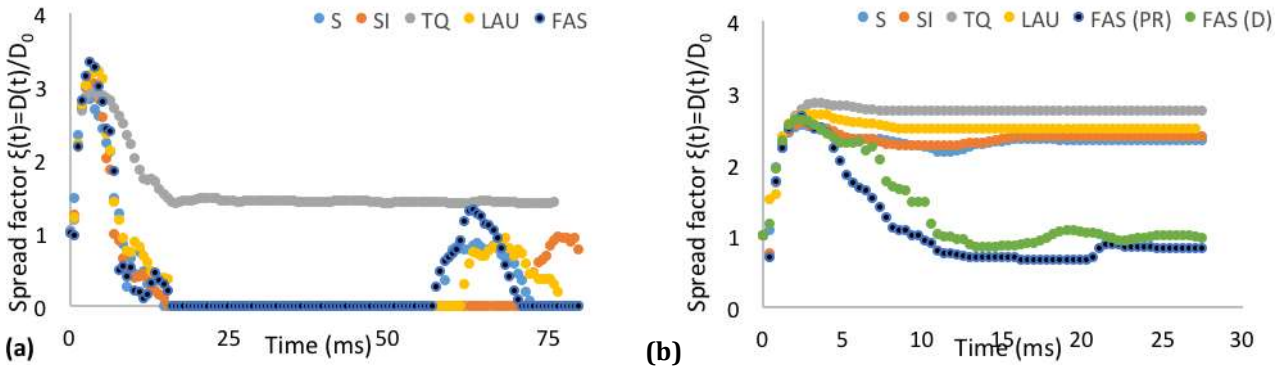

Figure 8. Spread factor time evolution, $\xi(t)=D(t)/D_o$, for the tested samples (single runs). (a) Water test conditions: V = 1.6 m/s, D_o = 2.5 mm, and We ≈ 90. (b) Hexadecane test conditions: V = 1.5 m/s, D_o = 1.7 mm, and We ≈110.

The fact that a surface is superhydrophobic, i.e. with an extremely high advancing contact angle and low hysteresis, is not enough to assure the complete rebound, since impalement can occur.[21] Therefore it is interesting to understand when the impalement impedes the bouncing and which are the possible outcomes of drop impact for the different fluid and surface characteristics. The impalement is usually described using alternatively four different pressure mechanisms, the water hammer pressure P_{WH}, the dynamic spreading pressure P_{SD}[31], the capillary or anti-wetting pressure P_C[32] and the gas layer pressure P_{GL}[22]. This last pressure term comes out considering the compression effects of the gas under the drop rather than the liquid compressibility. The initial impact of the droplet onto the surfaces generates a water hammer pressure P_{WH} due to the compression of the liquid[32-34]. The water hammer pressure P_{WH} is equal to $\rho_l CU$, where ρ_l is the droplet density, C is the velocity of sound in water, and U is the droplet impact velocity normal to the wall. Due to the complexity of the drop wall interaction, for example looking at the air entrainment, such water hammer pressure is usually reduced of a factor k, which has been experimentally evaluated lying in a very broad range, for example 0.2 by Deng et al.[33] or 0.002 by Maitra et al.[22] The real value of the impact pressure due to the liquid compressibility is here called effective water hammer pressure P_{EWH}. At the spreading stage, a liquid jump overtakes the outward moving contact line.[35] At this stage the spreading process implies a dynamic pressure $P_{SD} = 0.5\rho_l V^2$, where V is the spreading velocity. For a normal impact P_{EWH} is supposed to be greater than P_{SD}. The capillary pressure can be defined as the liquid pressure level that it is necessary to overcome in order to squeeze a droplet through a pore cavity, such as a surface topology throat. For that reason it is also called "anti-wetting" pressure. The capillary pressure can be written as $P_C \approx \sigma(-\cos\theta_A)/r_p$, where σ is the surface tension, θ_A is the advancing contact angle of the corresponding smooth surface and r_p is a length scale of the surface cavities. The analysis of droplet impact on textured surfaces showed that the compressibility of the air layer between droplet and the substrate is a key feature for the impalement. Maitra et al.[22] showed that the meniscus penetration is probably linked to the compressibility of the draining air, rather than the water hammer pressure effect of the liquid. Therefore, instead of the water hammer pressure, using a dimensional analysis they defined a pressure term $P_{GL} = 0.88(R\mu_g^{-1}U^7\rho_l^4\ Ca)^{1/3}/St^{4/9}$, where R is the droplet radius, μ_g the air viscosity, Ca the Capillary number, and St the Stokes number, as the critical pressure above which Cassie-to-Wenzel Transition occurs.

The impalement can be total, i.e. the liquid is reaching the bottom of the surface when the same is textured with pillars or is completely wetting the surface structure for a random topology, or partial, when the liquid is not able to wet completely and some air is still present in the surface throats and cavities. One can distinguished three regimes, the Wenzel regime where impalement occurs and is pre-

sent until the final deposition, being the liquid imbibed into the surface structure, a fakir (or Cassie-Baxter) regime, when no impalement and no imbibition occur for all the duration of the drop impact, from the early stages until the possible rebound or deposition, and a third stage, called partially impaled state, when a partial impalement is present. In the case $P_C > P_{EWH} > P_{SD}$, the surface textured structure resists wetting in the contact and in the spreading phase; in the case $P_{EWH} > P_C > P_{SD}$ the fluid penetrates during the contact stage. In the fakir state, for having a rebound as outcome of the drop impact is necessary that the liquid lamella is stretched enough to have sufficient energy at the end of the recoiling phase, thus promoting the drop detachment from the surface, i.e. it is necessary to have enough impact kinetic energy (the kinetic energy of the impinging droplet has to be larger than the surface energy dissipated during the retraction stage[31,36] (bouncing fakir droplet – B); otherwise the drop does not rebound (non-bouncing fakir state - NB). When the liquid meniscus penetrates the surface topology, the partially impaled state occurs: at low impact velocity a partially penetrated bouncing droplet state (PPB) occurs, instead at higher drop impact velocity, i.e. for a given critical velocity $U_{c,p}$, the so-called second non-bouncing droplet (2NB) state[32] occurs.

The main problem is that there is still an open debate on the criteria for impalement, since, if it is clear that impalement will appear when the anti-wetting pressure P_C is lower than a pressure linked to the impact dynamics, i.e. P_{EWH}, P_{GL} or P_{SD}, the actual threshold values are still unknown. Maitra et al.[47] suggested that $P_{GL} > 80\ P_C$ should be used as an impalement criterion, which impedes the complete rebound. From this expression the critical Weber number above which a complete rebound cannot occur can be evaluated: $We_{cr,imp} = 18.2 R^{1/2} \mu_g^{2/7} \rho_l^{-1/7} \sigma^{1/7} (\cos\theta_A)^{9/14} r_p^{-9/14}$. The smaller the cavity size, the higher must be the impact velocity above which also Cassie-to-Wenzel transition (CWT)[22,37] will occur. This is in qualitative agreement with the different output we observed at high We on surfaces with different morphologies: S and SI samples have nanoscale cavities on their surfaces, hence a $U_{c,p}$ higher ($We(U_{c,p}) > 620$) than the maximum U investigated in these experiments. Instead, LAU and FAS surfaces displayed only sub-micrometric voids which originated a smaller $U_{c,p}$ and therefore the CWT can be observed at We~550 for LAU and We~200 for FAS. However, it is very difficult to assess the critical Weber number for surfaces having a stochastic roughness, such as those used in the present work. $We_{cr,imp}$ and P_C are hard to determine due the length scale parameter for the surface cavities. Moreover, Quan and Zhang[38] demonstrated how the initial and operating conditions, including the microstructured superhydrophobic surfaces geometrical shapes will significantly influence the bouncing ability of an impinging droplet on textured surfaces.

Because the drop mobility is related to a sort of "dynamic superamphiphobicity", defined as the critical wetting value under which a complete drop rebound is observed, the critical impact velocity for having a dynamical amphiphobic surface is increasing with the surface tension, i.e., for the same advancing contact angles, a low surface tension fluid will have a lower threshold for impalement. Hence for a given impact velocity, a drop tends to deposit rather than to rebound when a lower surface tension fluid is involved. It is also important to stress that another important dimensionless number, the Ohnesorge number, i.e. the viscous dissipation, may influence the drop rebound. For water, the Ohnesorge number is about 0.0024, while for hexadecane is 7 times higher ($Oh_{Hex} \approx 0.0177$), therefore, the viscous dissipation prevents the liquid to rise back[41] from the partial penetration to a Cassie-Baxter regime. Since for our experiments the drop rebound is not possible to be achieved using hexadecane, the single effect of viscosity cannot be estimated. The rebound may therefore happen for a given impact velocity range $U_{r,min} < U < U_{r,max}$[31,39,40].

Finally in the present literature, the "chemistry" of the surface and of the liquid has never been considered a crucial factor for determining the CWT. However, it becomes clear that also the chemistry of the surface and the physico-chemical interactions with the liquid drops play an important role in determining $We_{cr,imp}$. For water drops with We = 150÷360, different outputs are observed for LAU and FAS surfaces notwithstanding their identical morphology (see Table 1 and Figures 2 and 8) and wettability (see Figure 1). The difference between these surfaces must lie in their chemical composition, as LAU is functionalized with non-polar alkyl chains while FAS exposes polar fluorinated groups. Murase and Fujibayashi[42] demonstrated that water forms hydrogen bonds with such fluorinated moieties on hydrophobic surfaces. Therefore, we may consider that these interactions cause kinetic energy dissipation in the drop. Nakajima et al.[43] calculated that this dissipation depends on the contact area between the drop and the surface. At We < 150, drop spreading is limited, thus water-surface contact area is small and the interaction negligible. Increasing impact speed, drop spreading and contact area become larger, therefore hydrogen bonds start to play a role causing dissipation and hindering rebound. When We > 500, water drops penetrate the terrace-like morphology of both LAU and FAS samples (e.g. partial rebound), therefore the role of chemistry is no longer relevant. Instead, for hexadecane drops, no influence of the surface chemistry can be recognized: the very low surface tension makes more probable to either splash at high We or deposit at low We, when the kinetic energy is insufficient to break the drop. Only a small influence of the surface structure is observed, causing the splash-deposition transition to shift to lower Weber values for the S and SI samples with a

flower-like surface morphology (Table 1). This is the first time that this influence of chemistry on the drop impact behavior on textured surfaces is reported. However, other explanation can be evoked as well, e.g. a more inhomogeneous grafting of FAS chains on unexposed parts of the surface topology with respect to LAU molecules. Static or quasi-static wetting measurements might not highlight such differences in surface chemical composition, while impinging drops could "touch" these areas and cause retention of the drop. As if a wettability gradient along the surface asperities is formed, that causes a different drop-surface interaction. Future work will extend the comprehension of such phenomena, possibly adding molecular dynamics modeling of the interactions between the surface and the drop.

CONCLUSIONS

The normal impact of water and hexadecane liquid drops onto dry, rigid surfaces with different wettabilities has been studied experimentally using a high-speed camera. The results highlighted that it is not possible to easily correlate contact angles (receding, advancing and hysteresis) and drop impact dynamics of low and high surface tension liquids on different surfaces. The Cassie-to-Wenzel transition can be observed even on statically repellent surfaces. In order to explain the observed phenomena, physical and chemical characteristics of both the liquid drops and the surface have to be taken into account. Surface morphology is crucial in defining the critical velocity over which impalement occurs: the smaller the surface cavities, the higher $U_{cr,imp}$. Also, surface chemistry as hydrogen bonding between surface functional groups and molecules in the liquid phase, can lower $U_{cr,imp}$ and favor impalement, as the wettability gradient along the surface asperities is relevant in determining the drop impact behavior. As far as the liquid properties are concerned, in agreement with Butt[39], with increasing viscosity and lower fluid surface tension the CWT shifts to smaller Weber numbers. In the case of hexadecane drops, the CWT threshold is so low that no rebound has been observed, even if the contact angles are well above the expected critical values obtained from previous works focusing on water drops. The effect of energy dissipation for high viscous fluids is therefore important when the liquid retreats from the texture[44,45]. Finally, it is clear that, at the moment, there is still a lack of an agreed general and quantitative evaluation of the impalement criteria after a drop impact. For example, the proposed thresholds in literature are not yet able to properly describe the results obtained using oils on amphiphobic surfaces.

A direct consequence of the study is linked to the numerical simulations of drop impacts onto rigid and dry surfaces. They consider the advancing and receding contact angles and surface tension in order to represent the impact outcomes[46]. A direct and important consequence of this study is that all the numerical simulations of drop impact onto solid, dry surfaces will never be able to capture the final outcome of the impact for all the possible fluids, if the surface topology and chemistry are not properly considered. Static or quasi-static wetting measurements might not highlight such differences in surface chemical composition. Furthermore, the present results emphasize how an accurate design of the surface properties must be pursued in the future research towards dynamically amphiphobic surfaces.

AUTHOR INFORMATION

Corresponding Author

*E-mail: m.marengo@brighton.ac.uk

Author Contributions

The manuscript was written through contributions of all authors. All authors have given approval to the final version of the manuscript.

ACKNOWLEDGMENTS

The authors acknowledge the European Cooperation in Science and Technology — MPNS COST Action MP1106 "Smart and green interfaces — from single bubbles and drops to industrial, environmental and biomedical applications" led by Prof. T. Karapantsios.

REFERENCES

1. Marengo, M.; Antonini, C.; Roisman, I. V.; Tropea, C. Drop collisions with simple and complex surfaces. *Curr. Opin. Colloid Interface Sci.* **2011**, 16, 292-302.
2. Bertola, V.; Wang, M. Dynamic contact angle of dilute polymer solution drops impacting on a hydrophobic surface. *Colloids Surf., A* **2015**, 481, 600-608.
3. Milionis, A.; Krishnan, K. G.; Loth, E. Hemolymph drop impact outcomes on surfaces with varying wettability. *App. Surf. Sci.* **2015**, 345, 36-43.
4. Malavasi, I.; Bernagozzi, I.; Antonini, C.; Marengo, M. Towards a standard protocol for assessing durability of superhydrophobic surfaces. *Surface Innovations* **2014**, 3, 49-60.
5. Feng, X. J.; Jiang, L. Design and Creation of Superwetting/Antiwetting Surfaces. *Adv. Mater.* **2006**, 18, 3063-3078.
6. Quéré, D. Non-sticking drops. Rep. *Prog. Phys.* **2005**, 68, 2495-2532.
7. Shirtcliffe, S. N. J.; McHale, G.; Atherton, S.; Newton, M. I. An introduction to superhydrophobicity. *Adv. Colloid Interface Sci.* **2010**, 161, 124-138.
8. Jiang, J. Y.; Xu, J. L.; Liu, Z.H.; Deng, L.; Sun, B.; Liu, S. D.; Wang, L.; Liu, H. Y. Preparation, corrosion resistance and hemocompatibility of the superhydrophobic TiO2 coatings on biomedical Ti-6Al-4V alloys. *App.Surf. Sci.* **2015**, 347, 591-595.
9. Crawford, R. J.; Ivanova, E. P. Biological Interactions with Superhydrophobic Surfaces. In *Superhydrophobic Surfaces*; Elsevier: 2015; pp 151-160.

10. Gogolides, E.; Ellinas, K.; Tserepi, A. Hierarchical micro and nano structured, hydrophilic, superhydrophobic and superoleophobic surfaces incorporated in microfluidics, microarrays and lab on chip microsystems. *Microelectron. Eng.* **2015**, 132, 135-155.
11. Zhang, F. Z.; Zhao, L. L.; Chen, H. Y.; Xu, S. L.; Evans, D. G.; Duan, X. Corrosion resistance of superhydrophobic layered double hydroxide films on aluminum. *Angew. Chem. Int. Ed.* **2008**, 47, 2500-2503.
12. Lee, C. Y.; Kim, C. J. Underwater restoration and retention of gases on superhydrophobic surfaces for drag reduction. *Phys. Rev. Lett.* **2011**, 106, 14502-14506.
13. Antonini, C.; Innocenti, M.; Horn, T.; Marengo, M.; Amirfazli, A. Understanding the effect of superhydrophobic coatings on energy reduction in anti-icing systems. *Cold Reg. Sci. Technol.* **2011**, 67, 58-67.
14. Genzer, J.; Efimenko, K. Recent developments in superhydrophobic surfaces and their relevance to marine fouling: a review. *Biofouling* **2006**, 22, 339-360.
15. Yuan, Y.; Lee, T.R. Contact Angle and Wetting Properties. In *Surface Science Techniques*; Bracco, G., Holst, B., Eds.; Springer Series in Surface Sciences 51; Springer: 2013; pp 3-34.
16. Cavalli, A.; Mugele, F. Superamphiphobic Surfaces. In *Droplet Wetting and Evaporation*; Brutin, D. Eds.; From Pure to Complex Fluids; Elsevier, Academic Press: Aix-Marseille University, France, 2015; pp 57-69.
17. Mou, C. Y.; Yuan, W. L.; Shih, C. H. Preparation and characterization of ultra-thin amphiphobic coatings on silicon wafers. *Thin Solid Films* **2013**, 423, 202-207.
18. Tsekov, R.; Borissov, D.; Karakashev, S. I. Wetting dynamics on lyophilic solid surfaces patterned by lyophobic islands. *Colloids Surf., A* **2013**, 77-80.
19. Wang, H.; Gao, D.; Meng, Y.; Wang, H.; Wang, E.; Zhu, Y. Corrosion-resistance, robust and wear-durable highly amphiphobic polymer based composite coating via a simple spraying approach. *Prog. Org. Coat.* **2015**, 82, 74-80.
20. Chua, Z.; Seeger, S. Superamphiphobic surfaces. *Chem. Soc. Rev.* **2014**, 43, 2784-2798.
21. Antonini, C.; Villa, F.; Bernagozzi, I.; Amirfazli, A.; Marengo, M. Drop Rebound after Impact: The Role of the Receding Contact Angle. *Langmuir* **2013**, 29, 16045-16050.
22. Maitra, T.; Tiwari, M. K.; Antonini, C.; Schoch, P.; Jung, S.; Eberle, P.; Poulikakos, D. On the Nanoengineering of Superhydrophobic and Impalement Resistant Surface Textures below the Freezing Temperature. *Nano Lett.* **2014**, 14, 172-182.
23. Roisman, I. V.; Lembach, A.; Tropea, C. Drop splashing induced by target roughness and porosity: The size plays no role. *Adv. Colloid. Interface Sci.* **2015**, 222, 615-621.
24. Raimondo, M.; Blosi, M.; Caldarelli, A.; Guarini, G.; Veronesi, F. Wetting behavior and remarkable durability of amphiphobic aluminum. *Chem. Eng. J.* **2014**, 258, 101-109.
25. Yang, S.; Qiu, R.; Song, H.; Wang, P.; Shi,Z.; Wang,Y. Slippery liquid-infused porous surface based on perfluorinatedlubricant/iron tetradecanoate: Preparation and corrosion protectionapplication. *App.Surf. Sci.* **2015**, 328, 491-500.
26. Charpentier, T. V. J.; Neville, A.; Baudin, S.; Smith, M. J.; Euvrard, M.; Bell, A.; Wang, C.; Barker, R. Liquid infused porous surfaces for mineral fouling mitigation. *J. Colloid Interface Sci.* **2015**, 444, 81–86.
27. Bernagozzi, I.; Antonini, C.; Villa, F.; Marengo, M. Fabricating superhydrophobic aluminum: an optimized one-step wet synthesis using fluoroalkyl silane. *Colloids Surf., A* **2014**, 441, 919-924.
28. Geometric Product Specifications (GPS) – Surface texture: Areal - Part 2: Terms, definitions and surface texture parameters. ISO 25178, April 01, 2012.
29. Antonini, C.; Amirfazli, A.; Marengo, M. Drop impact and wettability: from hydrophilic to superhydrophobic surfaces. *Phys. Fluids.* **2012**, 24, 102104-102113.
30. Bartolo, D.; Josserand, C.; Bonn, D. Singular Jets and Bubbles in Drop Impact. *PRL* **2006**, 96, 124501_1-4.
31. Bartolo, D.; Bouamrirene, F.; Verneuil, É.; Buguin, A.; Silberzan, P.; Moulinet, S. Bouncing or sticky droplets: Impalement transitions on superhydrophobic micropatterned surfaces. *Europhys. Lett.* **2006**, 74, 299-305.
32. Kwon, D. H.; Lee, S. J. Impact and wetting behaviors of impinging microdroplets on superhydrophobic textured surfaces. *Appl. Phys. Lett*. **2012**, 100, 171601_1-4
33. Deng, T.; Varanasi, K. K.; Hsu, H.; Bhate, N.; Keimel, C.; Stein, J.; Blohm, M. Nonwetting of impinging droplets on textured surfaces. *Appl. Phys. Lett*. **2009**, 94, 133109_1-3.
34. Moulinet, S.; Bartolo, D. Life and death of a fakir droplet: Impalement transitions on superhydrophobic surfaces. *Eur. Phys. J. E* **2007**, 24, 251-260.
35. Mandre, S.; Mani, M.; Brenner; M.P. Precursors to Splashing of Liquid Droplets on a Solid Surface. *PRL* **2009**, 102, 134502_1-4.
36. Reyssat, M.; Pépin, A.; Marty, F.; Chen, Y.; Quéré, D. Bouncing transitions on microtextured materials. *Europhys. Lett*. **2006**, 74, 306-312.
37. Antonini, C.; Lee. J. B.; Irvine, S.; Derome, D.; Tiwari, M. K.; Carmeliet, J.; Poulikakos, D. Unraveling wetting transition through surface textures with X-rays: Liquid meniscus penetration phenomena. *Sci. Rep.* **2014**, 4:4055, 1-6.
38. Quan, Y.; Zhang, L.Z. Numerical and Analytical Study of The Impinging and Bouncing Phenomena of Droplets on Superhydrophobic Surfaces with Microtextured Structures. *Langmuir* **2014**, 30, 11640-11649.
39. Deng, X.; Schellenberger, F.; Papadopoulos, P.; Vollmer, D.; Butt, H. J. Liquid Drops Impacting Superamphiphobic Coatings. *Langmuir* **2013**, 29, 7847-7856.
40. Schutzius, T. M.; Jung, S.; Maitra, T.; Eberle, P.; Antonini, C.; Stamatopoulos, C.; Poulikakos, D. Physics of Icing and Rational Design of Surfaces with Extraordinary Icephobicity. *Langmuir* **2015**, 31, 4807-4821.
41. Extrand, C. W. Forces, pressures and energies associated with liquid rising in nonuniform capillary tubes. *J. Colloid Interface Sci.* **2015**, 450, 135–140.
42. Murase, H.; Fujibayashi, T. Characterization of molecular interfaces in hydrophobic systems. *Prog. Org. Coat.* **1997**, 31, 97-104.
43. Nakajima, A.; Miyamoto, T.; Sakai, M.; Isobe, T.; Matsushita, S. Comparative study of the impact and sliding behavior of water droplets on two different hydrophobic silane coatings. *App.Surf. Sci.* **2014**, 292, 990-996.
44. Lee, J. B.; Lee, S. H. Dynamic Wetting and Spreading Characteristics of a Liquid Droplet Impinging on Hydrophobic Textured Surfaces. *Langmuir* **2011**, 27, 6565-6573.
45. Hyvaluoma, J.; Timonen, J. Impact states and energy dissipation in bouncing and non-bouncing droplets. *J. Stat. Mech.* **2009**, P06010+10.

46. Malgarinos, I.; Nikolopoulos, N.; Marengo, M.; Antonini, C.; Gavaises, M. VOF simulations of the contact angle dynamics during the drop spreading: standard models and a novel wetting force model. *Adv. Colloid. Interface Sci.* **2014**, 212, 1-20.

47. Maitra, T.; Tiwari, M.K.; Antonini, C.; Schoch, P.; Jung, S.; Eberle, P.; Poulikakos, D. Correction to On the Nanoengineering of Superhydrophobic and Impalement Resistant Surface Textures below the Freezing, Temperature, Nano Lett. 2014, 14 (1), 172–182. DOI: 10.1021/nl4037092

1 TOC Graphic

2

3